Molecular layer deposition of zeolitic imidazolate framework-8 films

Jorid Smets,[a,b,‡] Alexander John Cruz,[a,c,d,‡,†] Víctor Rubio-Giménez,[a] Max L. Tietze,[a] Dmitry E. Kravchenko,[a] Giel Arnauts,[a] Aleksander Matavž,[a] Nathalie Wauteraerts,[a] Min Tu,[a,§] Kristof Marcoen,[c] Inhar Imaz,[e] Daniel Maspoch,[e,g] Maxim Korytov,[d] Philippe M. Vereecken,[a,d] Steven De Feyter,[f] Tom Hauffman,[c] and Rob Ameloot[a,*]

[a] Center for Membrane Separations, Adsorption, Catalysis, and Spectroscopy (cMACS), KU Leuven - University of Leuven, Celestijnenlaan 200F, Leuven, 3001, Belgium

[b] Sustainable Energy, Air & Water Technology (DuEL), Department of Bioscience Engineering, University of Antwerp, Groenenborgerlaan 171, Antwerp, 2020, Belgium

[c] Research Group of Electrochemical and Surface Engineering, Department of Materials and Chemistry, Vrije Universiteit Brussel, Pleinlaan 2, Brussels, 1050, Belgium

[d] Imec, Kapeldreef 75, Leuven, 3001, Belgium

[e] Catalan Institute of Nanoscience and Nanotechnology (ICN2), CSIC and The Barcelona Institute of Science and Technology, Campus UAB, Bellaterra, Barcelona, 08193, Spain

[f] Department of Chemistry, Division of Molecular Imaging and Photonics, KU Leuven, Leuven, 3001, Belgium

[g] ICREA Pg. LluísCompanys23, Barcelona, 08010, Spain

ABSTRACT: Vapor-phase film deposition of metal-organic frameworks (MOFs) would facilitate the integration of these materials into electronic devices. We studied the vapor-phase layer-by-layer deposition of zeolitic imidazolate framework 8 (ZIF-8) by consecutive, self-saturating reactions of diethyl zinc, water, and 2-methylimidazole on a substrate. Two approaches were compared: (1) Direct ZIF-8 'molecular layer deposition' (MLD), which enables a nanometer-resolution thickness control and employs only self-saturating reactions, resulting in smooth films that are crystalline as-deposited, and (2) Two-step ZIF-8 MLD, in which crystallization occurs during a post-deposition treatment with additional linker vapor. The latter approach resulted in a reduced deposition time and an improved MOF quality, *i.e.*, increased crystallinity and probe molecule uptake, although the smoothness and thickness control were partially lost. Both approaches were developed in a modified atomic layer deposition reactor to ensure cleanroom compatibility.

Metal-organic frameworks (MOFs) are porous solids constructed from metal nodes connected by organic linkers. Because of their record specific surface areas, adsorption capacities, and dielectric/electronic properties, MOFs are of interest in catalysis,[1–4] gas storage,[5] molecular separations,[6,7] and electronic devices.[8–17] In electronics applications, conventional solvent-based synthesis methods may be disadvantageous due to corrosion, contamination, and surface tension effects.[13] In the absence of solvents and dissolved salts, these obstacles can be circumvented.[11,13,18–20] The MOF chemical vapor deposition (CVD) method, previously employed for the deposition of low-k dielectrics,[11] involves (1) the deposition of an oxide precursor layer followed by (2) exposure to linker vapor to form the MOF.[21] The conversion of the oxide layer into a porous MOF film results in a significant thickness expansion, often 10 × or more,[19,21–26] which makes thickness control in the nm-range challenging. Moreover, on some substrates, it is hard to obtain continuous MOF films below a critical metal oxide precursor thickness (e.g., < 3 nm for ZIF-8 growth on Si wafers).[27] For some applications, more precise control over the film thickness is desired.[19]

Molecular layer deposition (MLD) is based on consecutive, self-saturating surface reactions of vaporized precursors separated by inert gas purge streams.[28,29] The technique is closely related to atomic layer deposition (ALD) but uses at least one organic molecule as a building block. ALD is a staple in semiconductor processing, enabling coatings with excellent conformity, uniformity, and thickness control at the (sub-)nm-level.[30–32] Solution-based layer-by-layer deposition methods for MOFs based on alternatingly contacting a substrate with reactant solutions have been around for many years.[33,34] More recently, vapor-phase layer-by-layer deposition

methods for MOFs have been reported (**Table S1, Figure 1a**).[20,28,35–44] Salmi *et al.* demonstrated MLD of MOF-5, and later expanded this technique to IRMOF-8.[35,36] Lausund and Nilsen reported MLD of UiO-66, and subsequently extended their approach to the amino-functionalized and expanded variants of this MOF.[38,39,45] Karpinnen *et al.* showed crystalline as-deposited copper-terephthalate via MLD.[44,46] These pioneering studies show the viability of MOF-MLD, even though, in most cases, crystalline materials were obtained only after a post-deposition treatment.[35,36,38,39,45,47] Apart from porous MOFs, **Table S1** lists several non-porous coordination polymers that have been deposited by MLD directly in crystalline form.[40,46,48] In 2019, Han *et al.* reported a vapor-phase layer-by-layer deposition of HKUST-1. In this study, metallic copper was evaporated rather than deposited in a self-limiting fashion. Films were crystalline as-deposited, though a limited thickness control was obtained (40 nm at 2 cycles).[41] In 2020, Silva *et al.* reported the MLD of an Eu-based UiO-66 analog. Though crystallinity was obtained in the as-deposited state, diffraction peaks were only observed after a high number of cycles (> 1000).[49]

Herein, we report the MLD of ZIF-8 thin films by consecutive self-saturating reactions of vaporized diethyl zinc (DEZ), water, and 2-methylimidazole (HmIM). We studied two different approaches: (1) Direct ZIF-8 MLD, in which crystallinity is obtained in the as-deposited state (**Figure 1b**), and (2) Two-step ZIF-8 MLD, in which the MOF crystallizes during a post-treatment step (**Figure 1c**).

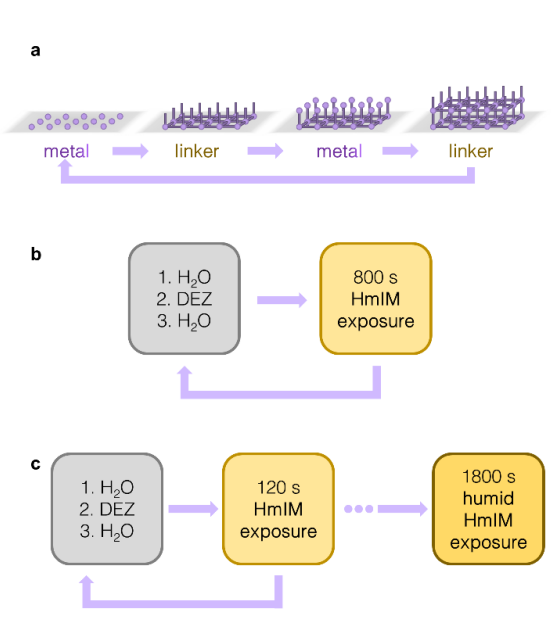

Figure 1. Schematic representation of ZIF-8 MLD. a) General representation of the vapor-phase layer-by-layer deposition. The protocols used for direct and two-step ZIF-8 MLD are shown in panels b and c, respectively.

Direct ZIF-8 MLD

An MLD protocol consists of reactant pulses separated by purge steps. In each cycle, sufficient reactant should be provided to complete the surface reaction. The purge steps should be long enough to remove all physisorbed (*i.e.*, non-reacted) precursor, though excessive purge steps will result in a lengthy process. In this work, a ZIF-8 MLD cycle comprises consecutively (1) deposition of a Zn-OH monolayer: first, H_2O pulses maximize the surface hydroxylation of the underlying layer to facilitate the reaction with the zinc precursor. Subsequently, DEZ pulses result in the deposition of a Zn-C_2H_5 monolayer. The next H_2O pulses remove the ethyl group, leaving a Zn-OH terminated surface. The formation of a Zn-OH monolayer is followed by (2) exposure to HmIM vapor to form ZIF-8. These steps are repeated to deposit a ZIF-8 film of a well-defined thickness at a growth rate of 9 Å/cycle. The crystallinity of the resulting films was confirmed by synchrotron grazing-incidence X-ray diffraction (GIXRD, **Figure 2a**), even for a single MLD cycle (**Figure S1**).

Ex-situ ellipsometry measurements of the deposited films after 10 cycles resulted in a modeled refractive index of 1.33 after activation at 100 °C in dynamic vacuum (λ = 633 nm), in line with values reported for ZIF-8 (1.30-1.38).[24,27,50] In addition, ellipsometry allows for monitoring the ZIF-8 MLD process *in-situ* and confirms the self-saturating behavior of the surface reactions (**Figure 2b,c**). In addition, these *in-situ* experiments revealed the relatively slow reaction kinetics and the need for a long HmIM pulse (800 s), even though the vapor pressure of HmIM is in the same order of magnitude as common ALD reactants (**Figure S2**).[51] For linker exposure times shorter than 400 s, no crystalline ZIF-8 films were obtained (**Figure S3**). Atomic force microscopy (AFM, **Figure 2d**) showed excellent surface coverage (RMS roughness 7.2 nm at 30 cycles), even at only three MLD cycles. The pinhole-free nature of the films was confirmed by conductive AFM measurements (**Figure S4**). If MOF-CVD was used instead, lower surface coverage was obtained for thin ZnO precursor layers (< 3 nm), as dispersed crystallites formed instead of a continuous film. This phenomenon can be explained by the increased mobility associated with longer linker exposure times (**Figure S5**).[22,27,52,53] The large-scale spatial uniformity of the ZIF-8 MLD films was verified by coating a 200 mm Si wafer with minimal thickness variation (29.5 ± 2.4 nm), as determined by *ex-situ* ellipsometry mapping, **Figure S6**.

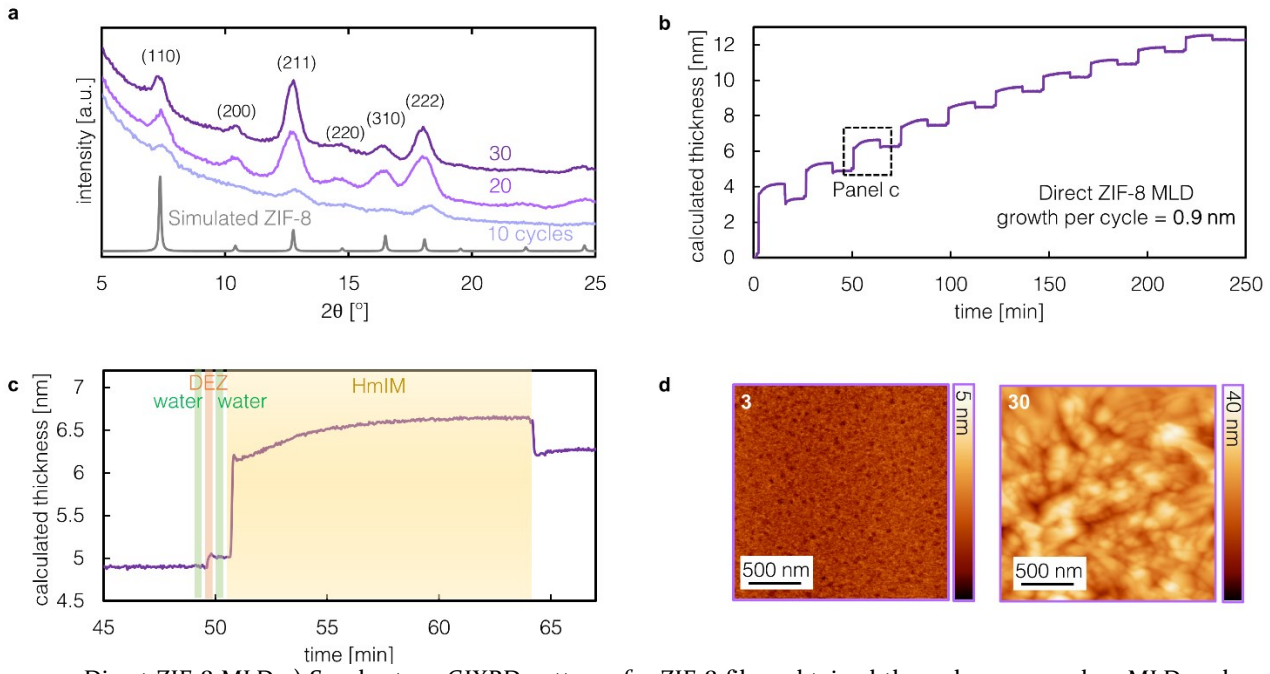

Figure 2. Direct ZIF-8 MLD a) Synchrotron GIXRD patterns for ZIF-8 films obtained through 10, 20, and 30 MLD cycles, compared to a simulated ZIF-8 diffractogram (CCDC code: VELVOY).[54] b) *In-situ* ellipsometry during direct ZIF-8 MLD deposition. Thickness from fitting the optical parameters of an extended Cauchy model after deposition, and using these constants to calculate the thickness as a function of time. The GPC is calculated starting from the third cycle to avoid deviations due to substrate interactions. c) Zoom of the *in-situ* ellipsometry data in panel (b). d) AFM measurements for 3 and 30 cycles of direct ZIF-8 MLD.

Water has multiple roles in the direct ZIF-8 MLD process: (1) generating Zn-OH moieties, resulting in a reactive surface, (2) protonating the linker,[55,56] hence rendering it susceptible to reaction with surface hydroxyls, and (3) promoting precursor mobility on the surface to aid crystallization.[57] Without a water pulse preceding the HmIM exposure, non-continuous ZIF-8 films were obtained due to the lower Zn-OH coverage (**Figure S7**). Removing both water pulses from the process resulted in amorphous films (**Figure S8**). Previous studies showed that CVD of ZIF-67, the Co^{2+}-equivalent of ZIF-8, is unsuccessful when water vapor is replaced by methanol or ethanol.[58,59] When the second water pulse in the ZIF-8 MLD process was replaced by methanol (*i.e.*, H_2O-DEZ-MeOH-HmIM), a crystalline yet rough and non-continuous ZIF-8 film was obtained (**Figure S9**, RMS roughness of 10.3 nm at 30 cycles) as the surface was covered with Zn-O-CH_3 and Zn-C_2H_5 instead of Zn-OH.[60] When both water pulses were replaced by methanol (*i.e.*, MeOH-DEZ-MeOH-HmIM), no crystalline ZIF-8 was formed (**Figure S9**).

Ellipsometric porosimetry using methanol as a probe molecule was used to evaluate the uptake properties of the ZIF-8 MLD films. These measurements indicate that, even though the ZIF-8 MLD films have crystalline domains, they are likely highly defective. Compared to solution-deposited films, the MLD films showed a much lower uptake, and the methanol isotherms lack the characteristic S-shape (**Figure S10b**), likely because of an abundance of Zn-OH defects. We found that the adsorption behavior of the films could be much improved through a post-deposition treatment step with humid HmIM vapor (1800 s), resulting in an increased methanol adsorption capacity and S-shaped isotherm (**Figure S10**). In contrast, only minor improvements in the crystallinity were observed (**Figure 3a**). We hypothesize that the post-treatment heals surface defects, thus improving the pore accessibility.

Two-step MOF-MLD

The direct MLD method is impractically slow (10 cycles take 4 h). Therefore, we tested a two-step ZIF-8 MLD approach (**Figure 1c**) with a much shorter linker exposure step during film growth (120 instead of 500 s) and reduced purge times (180 instead of 500 s) followed by post-deposition treatment with humid HmIM vapor. Since HmIM vapor pressure builds up slowly in in the linker canister, the linker concentration in the carrier gas is reduced when purging is shortened to 180 s. During the deposition stage, a non-crystalline film with the same composition as ZIF-8 is deposited at a rate of 6 Å/cycle (**Figure 3b**); crystallization occurs during the subsequent humid HmIM exposure. After the post-deposition treatment, a modeled thickness of around 27

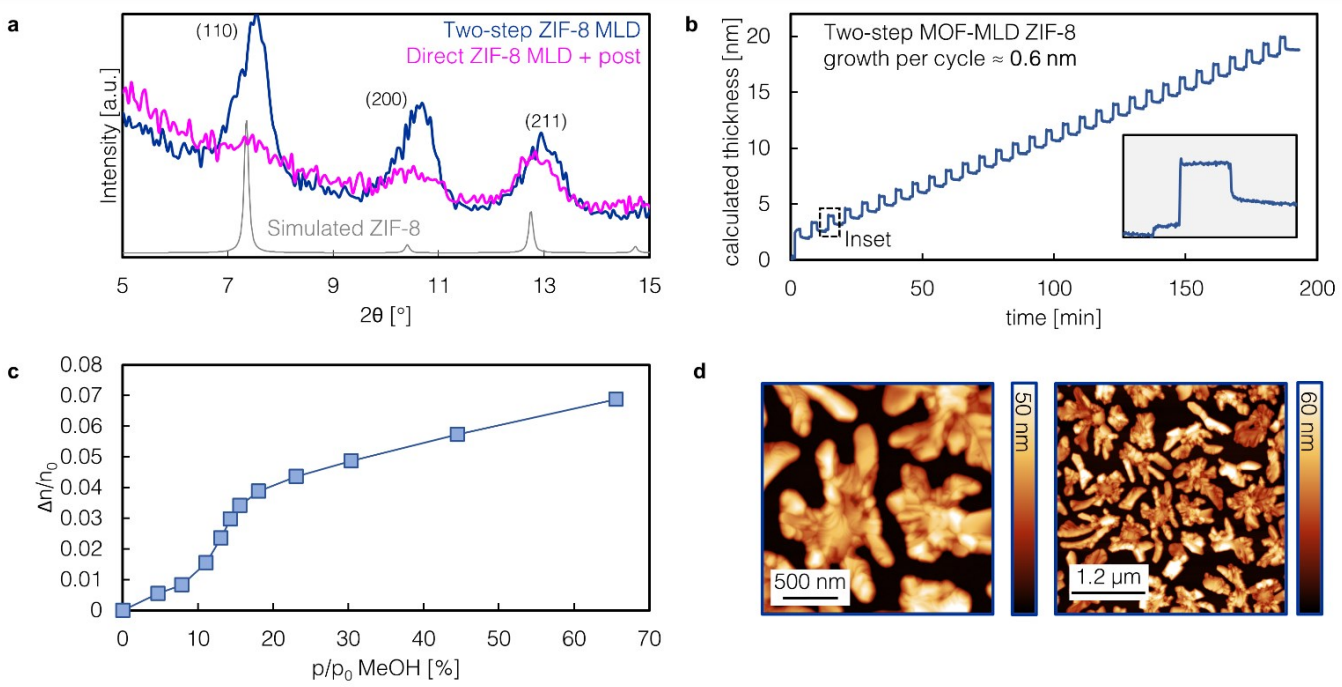

Figure 3. Two-step ZIF-8 MLD a) GIXRD comparing two-step ZIF-8 MLD (blue), and post-treated direct ZIF-8 MLD (pink). Both samples consist of 30 MLD cycles. b) *In-situ* ellipsometry during direct ZIF-8 MLD deposition, modelled as a Cauchy layer. Inset: 7-min time window. c) Ellipsometric porosimetry, modelled with an extended Cauchy model d) AFM of two-step ZIF-8 MLD on Si wafer.

nm is obtained (n is ~1.30 at 633 nm). The crystallinity (**Figure 3a**) and methanol adsorption capacity (**Figure 3c, S10c**) measured for these films were higher compared to films obtained through direct ZIF-8 MLD, even after post-deposition treatment: $\Delta n_{65.58\%}/n_o$(direct) = 0.013; $\Delta n_{65.58\%}/n_o$(direct + post) = 0.048, and $\Delta n_{65.58\%}/n_o$(two-step) = 0.069.

Hard X-ray photoelectron spectroscopy (HAXPES) using Ga K_α radiation was employed to study the ZIF-8 film properties because of the much larger inelastic mean free path length compared to Al K_α in XPS.[61] Therefore, HAXPES probes bulk rather than surface properties of nanometric films. HAXPES measurements show a N/Zn ratio of 3.6 for two-step ZIF-8 MLD, which is closer the ideal N/Zn of 4 than direct ZIF-8 MLD (N/Zn = 3.2), *i.e.*, there are fewer missing linkers in the framework (**Figure S11, S12**). Nevertheless, a defect sub-peak must be fitted when modeling the zinc and nitrogen peaks.[24] The defect fraction, defined as the intensity of the defect sub-peak relative to the total peak intensity, is higher for direct ZIF-8 MLD ($Zn_{defect}/Zn_{ZIF\text{-}8}+Zn_{defect}$ = 0.14, $N_{defect}/N_{ZIF\text{-}8}+N_{defect}$ = 0.14) than for two-step ZIF-8 MLD ($Zn_{defect}/Zn_{ZIF\text{-}8}+Zn_{defect}$ = 0.08, $N_{defect}/N_{ZIF\text{-}8}+N_{defect}$ = 0.06, **Figure S12**). Still, after storage in ambient air at room temperature for a few weeks, the crystallinity of the two-step MLD film dropped, and the methanol uptake and its characteristic isotherm shape disappeared (**Figure S13**). Degradation likely occurs through hydrolysis of the N-Zn bond and is faster for more defective films.

Mobility during HmIM exposure

For both direct ZIF-8 MLD and two-step ZIF-8 MLD, the HmIM post-deposition treatment improved the adsorption properties, but resulted in increased roughness due to Ostwald ripening (**Figure 3d, S10d,** RMS roughness 15.9 and 16.1 nm for direct MLD and two-step MLD after post-treatment, respectively). The fact that HmIM vapor exposure induces mobility in an existing ZIF layer could complicate the fabrication of MOF-on-MOF structures. These layered structures are recently gaining interest,[62] therefore to study this effect and assess the viability of depositions on existing ZIF frameworks, depositions were performed on (100)-oriented ZIF-8 supercrystals (**Figure S14a**).[63] Specular XRD was used to calculate the degree of crystallographic orientation as the peak intensity ratio of the (200) and (110) reflections. Due to the very low intensity of the (110) reflection for the oriented supercrystals, slight intensity changes in this peak will result in a significant variation of the (200)/(110) ratio. Therefore, this number is extremely sensitive to loss in crystalline orientation. Direct ZIF-8 MLD without a post-treatment step was used to avoid recrystallization of the supercrystal substrate. By depositing on an existing ZIF-8 framework (as with seeded growth methods), the local energetic barrier for crystal nucleation is lowered,[13] and the direct

MLD film quality is improved. When ZIF-8 CVD is performed on top of these crystals as a comparison, we observe that the crystalline orientation is lost due to recrystallization into a randomly oriented ZIF-8 (**Figure S14**). When direct ZIF-8 MLD is used, more of the orientation of the underlying substrate is maintained, though a decreasing trend with an increasing number of cycles is observed. To further characterize ZIF-8 MLD depositions on existing frameworks, conformality of the MOF-on-MOF coating was verified *via* SEM-EDX mapping of a ZIF-67 analog of the supercrystal substrate after MLD (**Figure S15-16**).

Conclusion

We show two approaches for ZIF-8 MLD, namely a direct method with nanometer-resolution thickness control where crystallinity is observed in the as-deposited state and a more practical two-step process that yields a higher MOF quality at a significantly shorter deposition time. These protocols expand the vapor-phase MOF deposition methods. We believe that MOF-MLD could be developed for all materials that can be deposited via MOF-CVD if there is an ALD precursor available to supply the metal without the need for strongly oxidizing co-reactants.

Methods

ZIF-8 MOF-MLD: The MOF-MLD ZIF-8 layers were deposited using deionized water (DIW), diethylzinc (DEZ, 97%, STREM), and freshly-ground HmIM (30 g, 99%, Sigma Aldrich) as precursors. Nitrogen (99.999%) was the carrier and purging gas used and sourced from a cleanroom header. Three 0.015 s pulses of DEZ in between two sets of three 0.015 s pulses of water were first dosed, separated by a purge duration of 5 s. This step was followed by HmIM exposure at stopped-flow conditions. In this step, the N_2 flow was stopped, and the outlet valve was closed, with an N_2 bubbler pressure of 110 mbar. As detailed in our previous work,[27] the bubbler-type sublimation vessel, supplied with 30 g of HmIM, was set to 125 °C, while the outlet and supply lines and the connections to the MOF reactor chamber were fixed to 130 °C and 135 °C, respectively. These lines were progressively heated in 30-minute intervals to prevent clogging during start-up. Before the depositions, purging and drying sequences (100 °C, 30 min) were implemented to ensure the removal of air in the headspace of the bottle and moisture/adsorbed water in the HmIM powder bed. The reactor base pressure during deposition was ~ 0.40 mbar at an N_2 gas flow of 20 sccm (manifold temperature: 150 °C). All depositions were carried out in a modified Savannah S-200 thermal ALD reactor (Veeco Instruments, Inc.) in an ISO 6 cleanroom (21 ± 1°C, relative humidity: 40 ± 5%). The different protocols mentioned in the main text (*i.e.*, direct MOF-MLD and two-step MOF-MLD) are schematically shown in **Figure S17** and **S18**. In all studied protocols, the importance of the thermal gradient in the reactor chamber has proven to be indispensable. The absence of or a diminished gradient resulted in an unsuccessful generation of ZIF-8 (**Figure S19**, **S20**).

Humidified conditions linker exposure: Immediately before dosing HmIM, ten additional water pulses were introduced in stopped-flow conditions, resulting in ~12% relative humidity (RH) in the reactor. This RH value was estimated by noting the pressure increase in the chamber after dosing, divided by the water saturation pressure at the reactor chamber temperature (80 °C).

MOF Activation protocol: The MLD recipes were terminated with an activation step. For this purpose, the N_2 flow was increased from 10 to 200 sccm. The vacuum was kept at 8.5 mbar as the substrate temperature was ramped up to 100°C and kept at this temperature. Since *in-situ* ellipsometry showed a constant profile after ~15 min (**Figure S21**), the activation sequence was terminated after 30 min.

ASSOCIATED CONTENT

The Supporting Information is available free of charge on the ACS Publications website:

Methods section (cont.); vapor-phase LBL deposition of MOFs in literature; synchrotron GIXRD at low number of cycles, Knudsen effusion measurements; effect of linker exposure time; c-AFM shows pinhole-free films; AFM of MOF-CVD with thin ZnO precursor layer; full-wafer ellipsometry mapping; direct ZIF-8 MLD with missing water pulse(s); (partially) substituting water with methanol; humidified conditions post-treatment of direct ZIF-8 MLD; HAXPES measurements; sample aging in lab air; deposition of oriented supercrystals; graphical illustration of direct and two-step ZIF-8 MLD protocols; need for a thermal gradient in the reactor chamber; ellipsometry during activation step; and ellipsometric porosimetry as a function of time (PDF)

AUTHOR INFORMATION

Corresponding Author

* E-mail: rob.ameloot@kuleuven.be

Present Addresses

† Baker Hughes, Schumanplein 6, Brussels 1040 Belgium
§ 2020 X-Lab and State Key Laboratory of Transducer Technology, Shanghai Institute of Microsystem and Information Technology, Chinese Academy of Sciences, Shanghai 200050, China

Author Contributions

‡ These authors contributed equally.

Notes

The authors declare no conflict of interest.

ACKNOWLEDGMENT

This project has received funding from the European Research Council (ERC) under the European Union's Horizon 2020 research and innovation program (grant agreement n° 716472, acronym VAPORE), from the Research Foundation Flanders (FWO Vlaanderen) in projects G085720N and G087422N, from VLAIO in project HBC.2020.2612, and from KU Leuven in project C14/20/085. The FWO Vlaanderen large-infrastructure project: HERCULES HAXPES (I014018N) is acknowledged. ICN2 is supported by the Severo Ochoa program from the Spanish MINECO (grant SEV-2017-0706). J.S., V.R.-G., G.A., M.T., N.W, and T.H. acknowledge the support of the FWO Vlaanderen for respectively the following fellowships: 11H8121N, 1263622N, 1SA7320N, 12ZK720N, 1SB7921N and 1295317N. D.E.K. acknowledges the Marie Sklodowska Curie Training Network HYCOAT, Grant Agreement 765378, for the financial support. The authors want to thank Mikhail Krishtab, Margot Verstreken, Sabina Rodríguez-Hermida, Michel De Cooman, Sammy W. Verbruggen, and Ivo Stassen for fruitful discussions. We gratefully acknowledge DELTA Dortmund synchrotron for the allocation of beamtime at beamline BL9 (proposal n° ID77) under the guidance of Christian Sternemann and Michael Paulus. We acknowledge Elettra Syncrotrone Trieste for providing access to its synchrotron radiation facilities (proposal n° 20180092, 20190028, 20200226, and 20210060) and thank Luisa Barba and Nicola Demitri for assistance in using beamline XRD1. The research leading to this result has been supported by the project CALIPSOplus under Grant Agreement 730872 from the EU Framework Programme for Research and Innovation HORIZON 2020.

ABBREVIATIONS

MOF, Metal-organic framework; MLD, Molecular layer deposition; ZIF, Zeolitic imidazolate framework; HmIM, 2-methyl imidazolate; DEZ, Diethyl zinc; CVD, Chemical vapor deposition; ALD, Atomic layer deposition; GPC, Growth per cycle; GIXRD, Grazing incidence X-ray diffraction; AFM, Atomic force microscopy; RMS, Root mean squared; HAXPES, Hard X-ray photoelectron spectroscopy; SEM-EDX, Scanning electron microscopy with energy dispersive x-ray analysis.

REFERENCES

(1) Lee, J.; Farha, O. K.; Roberts, J.; Scheidt, K. A.; Nguyen, S. T.; Hupp, J. T. Metal–Organic Framework Materials as Catalysts. *Chem. Soc. Rev.* **2009**, *38* (5), 1450–1459. https://doi.org/10.1039/B807080F.

(2) Furukawa, H.; Cordova, K. E.; O'Keeffe, M.; Yaghi, O. M. The Chemistry and Applications of Metal-Organic Frameworks. *Science* **2013**, *341* (6149), 1230444. https://doi.org/10.1126/science.1230444.

(3) Mueller, U.; Schubert, M.; Teich, F.; Puetter, H.; Schierle-Arndt, K.; Pastré, J. Metal–Organic Frameworks—Prospective Industrial Applications. *J. Mater. Chem.* **2006**, *16* (7), 626–636. https://doi.org/10.1039/B511962F.

(4) Czaja, A. U.; Trukhan, N.; Müller, U. Industrial Applications of Metal–Organic Frameworks. *Chem. Soc. Rev.* **2009**, *38* (5), 1284–1293. https://doi.org/10.1039/B804680H.

(5) Ma, S.; Zhou, H.-C. Gas Storage in Porous Metal-Organic Frameworks for Clean Energy Applications. *Chem. Commun.* **2010**, *46* (1), 44–53. https://doi.org/10.1039/B916295J.

(6) Li, X.; Liu, Y.; Wang, J.; Gascon, J.; Li, J.; Bruggen, B. V. der. Metal–Organic Frameworks Based Membranes for Liquid Separation. *Chem. Soc. Rev.* **2017**, *46* (23), 7124–7144. https://doi.org/10.1039/C7CS00575J.

(7) Ma, X.; Kumar, P.; Mittal, N.; Khlyustova, A.; Daoutidis, P.; Mkhoyan, K. A.; Tsapatsis, M. Zeolitic Imidazolate Framework Membranes Made by Ligand-Induced Permselectivation. *Science* **2018**, *361* (6406), 1008–1011. https://doi.org/10.1126/science.aat4123.

(8) Bétard, A.; Fischer, R. A. Metal–Organic Framework Thin Films: From Fundamentals to Applications. *Chem. Rev.* **2012**, *112* (2), 1055–1083. https://doi.org/10.1021/cr200167v.

(9) Kirchon, A.; Feng, L.; Drake, H. F.; Joseph, E. A.; Zhou, H.-C. From Fundamentals to Applications: A Toolbox for Robust and Multifunctional MOF Materials. *Chem. Soc. Rev.* **2018**, *47* (23), 8611–8638. https://doi.org/10.1039/C8CS00688A.

(10) Yoon, S. M.; Warren, S. C.; Grzybowski, B. A. Storage of Electrical Information in Metal–Organic-Framework Memristors. *Angew. Chem.* **2014**, *126* (17), 4526–4530. https://doi.org/10.1002/ange.201309642.

(11) Krishtab, M.; Stassen, I.; Stassin, T.; Cruz, A. J.; Okudur, O. O.; Armini, S.; Wilson, C.; De Gendt, S.; Ameloot, R. Vapor-Deposited Zeolitic Imidazolate Frameworks as Gap-Filling Ultra-Low-k Dielectrics. *Nat. Commun.* **2019**, *10* (1), 3729. https://doi.org/10.1038/s41467-019-11703-x.

(12) Talin, A. A.; Centrone, A.; Ford, A. C.; Foster, M. E.; Stavila, V.; Haney, P.; Kinney, R. A.; Szalai, V.; Gabaly, F. E.; Yoon, H. P.; Léonard, F.; Allendorf, M. D. Tunable Electrical Conductivity in Metal-Organic Framework Thin-Film Devices. *Science* **2014**, *343* (6166), 66–69. https://doi.org/10.1126/science.1246738.

(13) Stassen, I.; Burtch, N.; Talin, A.; Falcaro, P.; Allendorf, M.; Ameloot, R. An Updated Roadmap for the Integration of Metal–Organic Frameworks with Electronic Devices and Chemical Sensors. *Chem. Soc. Rev.* **2017**, *46* (11), 3185–3241. https://doi.org/10.1039/C7CS00122C.

(14) Tu, M.; Xia, B.; Kravchenko, D. E.; Tietze, M. L.; Cruz, A. J.; Stassen, I.; Hauffman, T.; Teyssandier, J.; De Feyter, S.; Wang, Z.; Fischer, R. A.; Marmiroli, B.; Amenitsch, H.; Torvisco, A.; Velásquez-Hernández, M. de J.; Falcaro, P.; Ameloot, R. Direct X-Ray and Electron-Beam Lithography of Halogenated Zeolitic Imidazolate Frameworks. *Nat. Mater.* **2021**, *20* (1), 93–99. https://doi.org/10.1038/s41563-020-00827-x.

(15) Allendorf, M. D.; Schwartzberg, A.; Stavila, V.; Talin, A. A. A Roadmap to Implementing Metal-Organic Frameworks in Electronic Devices: Challenges and Critical Directions. *Chemistry – Chem. Eur. J.* **2011**, *17* (41), 11372–11388. https://doi.org/10.1002/chem.201101595.

(16) Allendorf, M. D.; Dong, R.; Feng, X.; Kaskel, S.; Matoga, D.; Stavila, V. Electronic Devices Using Open Framework Materials. *Chem. Rev.* **2020**, *120* (16), 8581–8640. https://doi.org/10.1021/acs.chemrev.0c00033.

(17) Rubio-Giménez, V.; Tatay, S.; Martí-Gastaldo, C. Electrical Conductivity and Magnetic Bistability in Metal–Organic Frameworks and Coordination Polymers: Charge Transport and Spin Crossover at the Nanoscale. *Chem. Soc. Rev.* **2020**, *49* (15), 5601–5638. https://doi.org/10.1039/C9CS00594C.

(18) Friščić, T.; Halasz, I.; Beldon, P. J.; Belenguer, A. M.; Adams, F.; Kimber, S. A. J.; Honkimäki, V.; Dinnebier, R. E. Real-Time and in Situ Monitoring of Mechanochemical Milling Reac-

tions. *Nat. Chem.* **2013**, *5* (1), 66–73. https://doi.org/10.1038/nchem.1505.

(19) Su, P.; Tu, M.; Ameloot, R.; Li, W. Vapor-Phase Processing of Metal–Organic Frameworks. *Acc. Chem. Res.* **2022**, *55* (2), 186–196. https://doi.org/10.1021/acs.accounts.1c00600.

(20) Crivello, C.; Sevim, S.; Graniel, O.; Franco, C.; Pané, S.; Puigmartí-Luis, J.; Muñoz-Rojas, D. Advanced Technologies for the Fabrication of MOF Thin Films. *Mater. Horiz.* **2020**, 10.1039.D0MH00898B. https://doi.org/10.1039/D0MH00898B.

(21) Stassen, I.; Styles, M.; Grenci, G.; Gorp, H. V.; Vanderlinden, W.; Feyter, S. D.; Falcaro, P.; Vos, D. D.; Vereecken, P.; Ameloot, R. Chemical Vapour Deposition of Zeolitic Imidazolate Framework Thin Films. *Nat. Mater.* **2016**, *15* (3), 304–310. https://doi.org/10.1038/nmat4509.

(22) Stassin, T.; Stassen, I.; Marreiros, J.; Cruz, A. J.; Verbeke, R.; Tu, M.; Reinsch, H.; Dickmann, M.; Egger, W.; Vankelecom, I. F. J.; De Vos, D. E.; Ameloot, R. Solvent-Free Powder Synthesis and MOF-CVD Thin Films of the Large-Pore Metal–Organic Framework MAF-6. *Chem. Mater.* **2020**, *32* (5), 1784–1793. https://doi.org/10.1021/acs.chemmater.9b03807.

(23) Stassin, T.; Stassen, I.; Wauteraerts, N.; Cruz, A. J.; Kräuter, M.; Coclite, A. M.; De Vos, D.; Ameloot, R. Solvent-Free Powder Synthesis and Thin Film Chemical Vapor Deposition of a Zinc Bipyridyl-Triazolate Framework. *EurJIC* **2020**, *2020* (1), 71–74. https://doi.org/10.1002/ejic.201901051.

(24) Tietze, M. L.; Obst, M.; Arnauts, G.; Wauteraerts, N.; Rodríguez-Hermida, S.; Ameloot, R. Parts-per-Million Detection of Volatile Organic Compounds via Surface Plasmon Polaritons and Nanometer-Thick Metal–Organic Framework Films. *ACS Appl. Nano Mater.* **2022**, acsanm.2c00012. https://doi.org/10.1021/acsanm.2c00012.

(25) Tu, M.; Kravchenko, D. E.; Xia, B.; Rubio-Giménez, V.; Wauteraerts, N.; Verbeke, R.; Vankelecom, I. F. J.; Stassin, T.; Egger, W.; Dickmann, M.; Amenitsch, H.; Ameloot, R. Template-Mediated Control over Polymorphism in the Vapor-Assisted Formation of Zeolitic Imidazolate Framework Powders and Films. *Angew. Chem., Int. Ed.* **2021**, *60* (14), 7553–7558. https://doi.org/10.1002/anie.202014791.

(26) Rubio-Giménez, V.; Arnauts, G.; Wang, M.; Oliveros Mata, E. S.; Huang, X.; Lan, T.; Tietze, M. L.; Kravchenko, D. E.; Smets, J.; Wauteraerts, N.; Khadiev, A.; Novikov, D. V.; Makarov, D.; Dong, R.; Ameloot, R. Chemical Vapor Deposition and High-Resolution Patterning of a Highly Conductive Two-Dimensional Coordination Polymer Film. *J. Am. Chem. Soc.* **2023**, *145* (1), 152–159. https://doi.org/10.1021/jacs.2c09007.

(27) Cruz, A. J.; Stassen, I.; Krishtab, M.; Marcoen, K.; Stassin, T.; Rodríguez-Hermida, S.; Teyssandier, J.; Pletincx, S.; Verbeke, R.; Rubio-Giménez, V.; Tatay, S.; Martí-Gastaldo, C.; Meersschaut, J.; Vereecken, P. M.; De Feyter, S.; Hauffman, T.; Ameloot, R. Integrated Cleanroom Process for the Vapor-Phase Deposition of Large-Area Zeolitic Imidazolate Framework Thin Films. *Chem. Mater.* **2019**, *31* (22), 9462–9471. https://doi.org/10.1021/acs.chemmater.9b03435.

(28) Ahvenniemi, E.; Karppinen, M. *In Situ* Atomic/Molecular Layer-by-Layer Deposition of Inorganic-Organic Coordination Network Thin Films from Gaseous Precursors. *Chem. Mater.* **2016**, *28* (17), 6260–6265. https://doi.org/10.1021/acs.chemmater.6b02496.

(29) Sundberg, P.; Karppinen, M. Organic and Inorganic–Organic Thin Film Structures by Molecular Layer Deposition: A Review. *Beilstein J. Nanotechnol.* **2014**, *5* (1), 1104–1136. https://doi.org/10.3762/bjnano.5.123.

(30) Elam, J. W.; Routkevitch, D.; Mardilovich, P. P.; George, S. M. Conformal Coating on Ultrahigh-Aspect-Ratio Nanopores of Anodic Alumina by Atomic Layer Deposition. *Chem. Mater.* **2003**, *15* (18), 3507–3517. https://doi.org/10.1021/cm030308o.

(31) Meng, X. An Overview of Molecular Layer Deposition for Organic and Organic–Inorganic Hybrid Materials: Mechanisms, Growth Characteristics, and Promising Applications. *J. Mater. Chem. A* **2017**, *5* (35), 18326–18378. https://doi.org/10.1039/C7TA04449F.

(32) Johnson, R. W.; Hultqvist, A.; Bent, S. F. A Brief Review of Atomic Layer Deposition: From Fundamentals to Applications. *Mater. Today* **2014**, *17* (5), 236–246. https://doi.org/10.1016/j.mattod.2014.04.026.

(33) Shekhah, O.; Wang, H.; Kowarik, S.; Schreiber, F.; Paulus, M.; Tolan, M.; Sternemann, C.; Evers, F.; Zacher, D.; Fischer, R. A.; Wöll, C. Step-by-Step Route for the Synthesis of Metal–Organic Frameworks. *J. Am. Chem. Soc.* **2007**, *129* (49), 15118–15119. https://doi.org/10.1021/ja076210u.

(34) Shekhah, O.; Eddaoudi, M. The Liquid Phase Epitaxy Method for the Construction of Oriented ZIF-8 Thin Films with Controlled Growth on Functionalized Surfaces. *Chem. Commun.* **2013**, *49* (86), 10079. https://doi.org/10.1039/c3cc45343j.

(35) Salmi, L. D.; Heikkilä, M. J.; Vehkamäki, M.; Puukilainen, E.; Ritala, M.; Sajavaara, T. Studies on Atomic Layer Deposition of IRMOF-8 Thin Films. *J. Vac. Sci. Technol. A* **2014**, *33* (1), 01A121. https://doi.org/10.1116/1.4901455.

(36) Salmi, L.; Heikkilä, M.; Puukilainen, E.; Sajavaara, T.; Grosso, D.; Ritala, M. Studies on Atomic Layer Deposition of MOF-5 Thin Films. *Microporous and Mesoporous Mater.* **2013**, *182*, 147–154. https://doi.org/10.1016/j.micromeso.2013.08.024.

(37) Ahvenniemi, E.; Karppinen, M. Atomic/Molecular Layer Deposition: A Direct Gas-Phase Route to Crystalline Metal–Organic Framework Thin Films. *Chem. Comm.* **2016**, *52* (6), 1139–1142. https://doi.org/10.1039/C5CC08538A.

(38) Lausund, K. B.; Nilsen, O. All-Gas-Phase Synthesis of UiO-66 through Modulated Atomic Layer Deposition. *Nat. Commun.* **2016**, *7* (1), 13578. https://doi.org/10.1038/ncomms13578.

(39) Lausund, K. B.; Petrovic, V.; Nilsen, O. All-Gas-Phase Synthesis of Amino-Functionalized UiO-66 Thin Films. *Dalton Trans.* **2017**, *46* (48), 16983–16992. https://doi.org/10.1039/C7DT03518G.

(40) Tanskanen, A.; Karppinen, M. Iron-Terephthalate Coordination Network Thin Films Through In-Situ Atomic/Molecular Layer Deposition. *Sci. Rep* **2018**, *8* (1), 8976. https://doi.org/10.1038/s41598-018-27124-7.

(41) Han, S.; Ciufo, R. A.; Meyerson, M. L.; Keitz, B. K.; Mullins, C. B. Solvent-Free Vacuum Growth of Oriented HKUST-1 Thin Films. *J. Mater. Chem. A* **2019**, *7* (33), 19396–19406. https://doi.org/10.1039/C9TA05179A.

(42) Multia, J.; Karppinen, M. Atomic/Molecular Layer Deposition for Designer's Functional Metal–Organic Materials. *Adv. Mater. Interfaces* **2022**, *9* (15), 2200210. https://doi.org/10.1002/admi.202200210.

(43) Han, S.; Ciufo, R. A.; Wygant, B. R.; Keitz, B. K.; Mullins, C. B. Methanol Oxidation Catalyzed by Copper Nanoclusters Incorporated in Vacuum-Deposited HKUST-1 Thin Films. *ACS Catal.* **2020**, *10* (9), 4997–5007. https://doi.org/10.1021/acscatal.0c00592.

(44) Multia, J.; Kravchenko, D. E.; Rubio-Giménez, V.; Philip, A.; Ameloot, R.; Karppinen, M. Nanoporous Metal–Organic Framework Thin Films Prepared Directly from Gaseous Precursors by Atomic and Molecular Layer Deposition: Implications for Microelectronics. *ACS Appl. Nano Mater.* **2023**, *6* (2), 827–831. https://doi.org/10.1021/acsanm.2c04934.

(45) Lausund, K. B.; Olsen, M. S.; Hansen, P.-A.; Valen, H.; Nilsen, O. MOF Thin Films with Bi-Aromatic Linkers Grown by Molecular Layer Deposition. *J. Mater. Chem. A* **2020**, *8* (5), 2539–2548. https://doi.org/10.1039/C9TA09303F.

(46) Ahvenniemi, E.; Karppinen, M. Atomic/Molecular Layer Deposition: A Direct Gas-Phase Route to Crystalline Metal–Organic Framework Thin Films. *Chem. Commun.* **2016**, *52* (6), 1139–1142. https://doi.org/10.1039/C5CC08538A.

(47) Medishetty, R.; Zhang, Z.; Sadlo, A.; Cwik, S.; Peeters, D.; Henke, S.; Mangayarkarasi, N.; Devi, A. Fabrication of Zinc-Dicarboxylate- and Zinc-Pyrazolate-Carboxylate-Framework Thin Films through Vapour–Solid Deposition. *Dalton Trans.* **2018**, *47* (40), 14179–14183. https://doi.org/10.1039/C8DT00352A.

(48) Khayyami, A.; Philip, A.; Karppinen, M. Atomic/Molecular Layer Deposited Iron–Azobenzene Framework Thin Films for Stimuli-Induced Gas Molecule Capture/Release. *Angew. Chem., Int. Ed.* **2019**, *58* (38), 13400–13404. https://doi.org/10.1002/anie.201908164.

(49) Silva, R. M.; Carlos, L. D.; Rocha, J.; Silva, R. F. Luminescent Thin Films of Eu-Bearing UiO-66 Metal Organic Framework Prepared by ALD/MLD. *Applied Surface Science* **2020**, *527*, 146603. https://doi.org/10.1016/j.apsusc.2020.146603.

(50) Tao, J.; Wang, X.; Sun, T.; Cai, H.; Wang, Y.; Lin, T.; Fu, D.; Ting, L. L. Y.; Gu, Y.; Zhao, D. Hybrid Photonic Cavity with Metal-Organic Framework Coatings for the Ultra-Sensitive Detection of Volatile Organic Compounds with High Immunity to Humidity. *Sci. Rep.* **2017**, *7* (1), 41640. https://doi.org/10.1038/srep41640.

(51) Alfonso, F.; English, T. ALD Precursor Delivery & Debugging: A Case Study in Polymer Development. https://snfexfab.stanford.edu/docs/presentation/ald-precursor-delivery-debugging-case-study-in-polymer-development-final-presentation (accessed on 2022/04/05).

(52) Kräuter, M.; Cruz, A. J.; Stassin, T.; Rodríguez-Hermida, S.; Ameloot, R.; Resel, R.; Coclite, A. M. Influence of Precursor Density and Conversion Time on the Orientation of Vapor-Deposited ZIF-8. *Crystals* **2022**, *12* (2), 217. https://doi.org/10.3390/cryst12020217.

(53) Kwon, H. T.; Jeong, H.-K.; Lee, A. S.; An, H. S.; Lee, T.; Jang, E.; Lee, J. S.; Choi, J. Defect-Induced Ripening of Zeolitic-Imidazolate Framework ZIF-8 and Its Implication to Vapor-Phase Membrane Synthesis. *Chem. Commun.* **2016**, *52* (78), 11669–11672. https://doi.org/10.1039/C6CC05433A.

(54) Park, K. S.; Ni, Z.; Cote, A. P.; Choi, J. Y.; Huang, R.; Uribe-Romo, F. J.; Chae, H. K.; O'Keeffe, M.; Yaghi, O. M. CCDC 602542: Experimental Crystal Structure Determination. https://doi.org/10.5517/CCN6ZVN (accessed on 2021/12/21), 2006.

(55) Cliffe, M. J.; Mottillo, C.; Stein, R. S.; Bučar, D.-K.; Friščić, T. Accelerated Aging: A Low Energy, Solvent-Free Alternative to Solvothermal and Mechanochemical Synthesis of Metal–Organic Materials. *Chem. Sci.* **2012**, *3* (8), 2495–2500. https://doi.org/10.1039/C2SC20344H.

(56) Mottillo, C.; Lu, Y.; Pham, M.-H.; Cliffe, M. J.; Do, T.-O.; Friščić, T. Mineral Neogenesis as an Inspiration for Mild, Solvent-Free Synthesis of Bulk Microporous Metal-Organic Frameworks from Metal (Zn, Co) Oxides. *Green Chem.* **2013**, *15* (8), 2121–2131. https://doi.org/10.1039/C3GC40520F.

(57) Marreiros, J.; Dommelen, L. V.; Fleury, G.; Oliveira-Silva, R. de; Stassin, T.; Iacomi, P.; Furukawa, S.; Sakellariou, D.; Llewellyn, P. L.; Roeffaers, M.; Ameloot, R. Vapor-Phase Linker Exchange of the Metal–Organic Framework ZIF-8: A Solvent-Free Approach to Post-Synthetic Modification. *Angew. Chem., Int. Ed.* **2019**, *58* (51), 18471–18475. https://doi.org/10.1002/anie.201912088.

(58) Huang, J.-K.; Saito, N.; Cai, Y.; Wan, Y.; Cheng, C.-C.; Li, M.; Shi, J.; Tamada, K.; Tung, V. C.; Li, S.; Li, L.-J. Steam-Assisted Chemical Vapor Deposition of Zeolitic Imidazolate Framework. *ACS Materials Lett.* **2020**, 485–491. https://doi.org/10.1021/acsmaterialslett.0c00026.

(59) Shi, Q.; Chen, Z.; Song, Z.; Li, J.; Dong, J. Synthesis of ZIF-8 and ZIF-67 by Steam-Assisted Conversion and an Investigation of Their Tribological Behaviors. *Angew. Chem., Int. Ed.* **2011**, *50* (3), 672–675. https://doi.org/10.1002/anie.201004937.

(60) Herold, R. J.; Aggarwal, S. L.; Neff, V. MECHANISMS OF THE REACTIONS OF DIETHYLZINC WITH ISOPROPANOL AND WATER. *Can. J. Chem.* **1963**, *41* (5), 1368–1380. https://doi.org/10.1139/v63-187.

(61) Regoutz, A.; Mascheck, M.; Wiell, T.; Eriksson, S. K.; Liljenberg, C.; Tetzner, K.; Williamson, B. A. D.; Scanlon, D. O.; Palmgren, P. A Novel Laboratory-Based Hard X-Ray Photoelectron Spectroscopy System. *Rev. Sci. Instrum.* **2018**, *89* (7), 073105. https://doi.org/10.1063/1.5039829.

(62) Liu, C.; Wang, J.; Wan, J.; Yu, C. MOF-on-MOF Hybrids: Synthesis and Applications. *Coord. Chem. Rev.* **2021**, *432*, 213743. https://doi.org/10.1016/j.ccr.2020.213743.

(63) Avci, C.; Liu, Y.; Pariente, J. A.; Blanco, A.; Lopez, C.; Imaz, I.; Maspoch, D. Template-Free, Surfactant-Mediated Orientation of Self-Assembled Supercrystals of Metal–Organic Framework Particles. *Small* **2019**, *15* (31), 1902520. https://doi.org/10.1002/smll.201902520.

Table of Contents